tions. It is planned to present solutions to the equations containing higher degree terms in future papers.

Derivation of the Solution

The radial equation of motion in two-body theory is given as

$$\ddot{r} + \mu/r^2 - \mu a(1 - e^2)/r^3 = 0$$

By proper selection of the system of units, one may set the gravitational constant μ and the major semiaxis a both equal to 1. In this system, the angle traversed in unit time over a circular orbit of unit radius is 1 rad. Then,

$$\ddot{r} + 1/r^2 - (1 - e^2)/r^3 = 0\dagger \qquad (1)$$

where e is the eccentricity. Let

$$r = r_0 + \Delta r \qquad \Delta r/r_0 = \alpha$$

Then,

$$1/r^2 = 1/r_0^2(1 - 2\alpha)$$

neglecting terms of higher degrees, and

$$1/r^3 = 1/r_0^3(1 - 3\alpha) \qquad \ddot{r} = \Delta\ddot{r} = r_0\ddot{\alpha}$$

Then, from Eq. (1),

$$\ddot{\alpha} + \frac{1 - 2\alpha}{r_0^3} - \frac{(1 - e^2)(1 - 3\alpha)}{r_0^4} = 0 \qquad (2)$$

Rearranging terms,

$$\ddot{\alpha} + \left[\frac{3(1 - e^2)}{r_0^4} - \frac{2}{r_0^3}\right]\alpha = \frac{(1 - e^2)}{r_0^4} - \frac{1}{r_0^3}$$

Let

$$\omega^2 = 3(1 - e^2)/r_0^4 - 2/r_0^3 \qquad (2.1a)$$

or

$$\omega^2 = 2/r_0^3 - 3(1 - e^2)/r_0^4 \qquad (2.1b)$$

so that $\omega^2 > 0$;

$$C = (1 - e^2)/r_0^4 - 1/r_0^3 = \tfrac{1}{3}(\pm\omega^2 - 1/r_0^3)$$

(Note that ω is positive, a frequency or growth-decay rate.) Then the solution to (2) is

$$\alpha = 2C/\omega^2 \sin^2\omega t/2 + \dot{r}_0/(\omega r_0)\sin\omega t \qquad (3a)$$

$$\alpha = -2C/\omega^2 \sinh^2\omega t/2 + \dot{r}_0/(\omega r_0)\sinh\omega t \qquad (3b)$$

When $\omega = 0$, Eqs. (3) reduce to

$$\alpha = (\dot{r}_0 t/r_0) + \tfrac{1}{6}t^2/r_0^3 + \ldots$$

in the circular function case, and reduce to

$$\alpha = (\dot{r}_0 t/r_0) - \tfrac{1}{6}t^2/r_0^3 + \ldots$$

by the use of hyperbolic functions. Of course, since Δr was assumed small, one could not expect agreement past the first-degree term in a rectilinear case.

In order for orbits to have solutions of type (3b), one finds that the condition (2.1b) implies $r_0 \geq \frac{3}{2}(1 - e^2)$. Inasmuch as r_0 attains a maximum value of $1 + e$,‡ one finds that $1 + e \geq \frac{3}{2}(1 - e^2)$, or $e \geq \frac{1}{3}$. That is, (3b) will not occur as a solution unless $e \geq \frac{1}{3}$.

A simple check of Eq. (3a) can be made for small e by taking periapsis as starting point. Here,

$$r_0 = 1 - e \qquad \dot{r}_0 = 0$$

$$\omega^2 = \frac{1 + 3e}{(1 - e)^3} \qquad C = \frac{e}{(1 - e)^3}$$

and one has

$$\alpha = \frac{2e}{1 + 3e}\sin^2\left[\frac{1 + 3e}{(1 - e)^3}\right]^{1/2}\frac{t}{2} \qquad (4)$$

One knows, for example, that at apapsis ($t = \pi$), α must equal $2e/(1 - e)$. Equation (4), therefore, yields a fair approximation even in this extreme case, being correct to the first degree in e.

The change in true anomaly v from initial value v_0 is given by the expression relating angular momentum magnitude h to dv/dt§:

$$dv/dt = h/r^2$$

Since

$$h = [\mu a(1 - e^2)]^{1/2} = (1 - e^2)^{1/2}$$

one has

$$\frac{dv}{dt} = \frac{(1 - e^2)^{1/2}}{r^2}$$

therefore

$$v - v_0 = (1 - e^2)^{1/2}\int_{t_0}^{t}\frac{dt^*}{r^2}$$

This integral is approximated as follows:

$$\frac{1}{r^2} = \frac{1}{r_0^2}(1 - 2\alpha)$$

$$v - v_0 = \frac{[1 - e^2]^{1/2}}{r_0^2}\int_{t_0}^{t} dt^*(1 - 2\alpha)$$

Using (3a) for α in the foremention integral gives, for example,

$$v - v_0 = \frac{(1 - e^2)^{1/2}}{r_0^2}\left\{(t - t_0) - 2\left[\frac{C}{\omega^2}(t - t_0) - \frac{C}{\omega^3}(\sin\omega t - \sin\omega t_0) - \frac{\dot{r}_0}{\omega^2 r_0}(\cos\omega t - \cos\omega t_0)\right]\right\}$$

† In hyperbolic orbits, read $\ddot{r} + 1/r^2 - (e^2 - 1)/r^3 = 0$.

‡ Apapsis, elliptic orbits only.

§ Conventional methods may be more suitable (Kepler, Barker, Gauss).

Initial Evaluation of Perforated Ion Engine Emitters

J. J. Krauss* and E. N. Petrick†
Kelsey Hayes Company, Romulus, Mich.

In the continuing engineering development aimed toward the improvement of lifetime and reliability in ion engines, the emitter remains one of the critical areas. Inasmuch as the prospective missions require that the emitter function for thousands of hours at high temperatures, an engineering program has been initiated to determine the feasibility and characteristics of emitters made from thin solid plates into

Presented at the AIAA Electric Propulsion Conference, Colorado Springs, Colo., March 11–13, 1963; revision received August 2, 1963. Supported by Aeronautical Systems Division, U. S. Air Force, Contract No. AF 33(657)-8638.

* Senior Research Engineer.

† Chief Research Engineer. Associate Fellow Member AIAA.

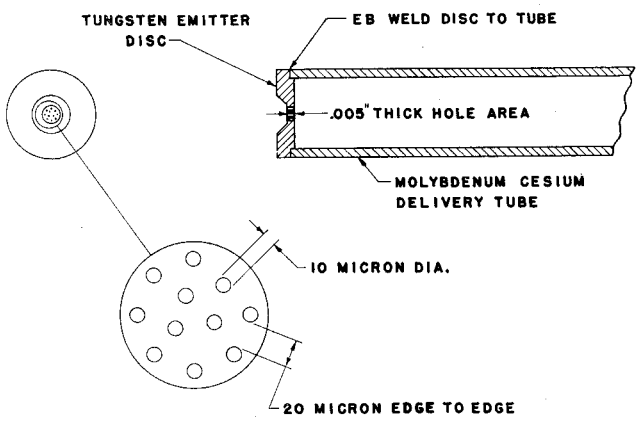

Fig. 1 Test emitter design.

which holes of the correct dimension have been placed. This type of emitter promises to be more durable and also more precise in regard to hole location and spacing than the conventional sintered powder disk or strip. In the present paper, a brief report is given on progress to date in evaluating such emitters with regard to durability and cesium flow characteristics.

An initial test emitter design was selected which is a compromise between the theoretical hole size required (as indicated by such analyses as given in Refs. 1 and 2, for example) and the present limits of manufacturing technology.

Pore sizes as low as 2μ were used in some phases of the tests.[3] In general, 10μ was the target pore diameter, as shown in Fig. 1.

Inert Gas Flow Tests

Prior to high-temperature cesium flow testing, a series of low pressure inert gas (nitrogen) flow tests were performed to check the validity of flow calculation techniques and also to provide a measure of the effects of operation with cesium (by comparative before and after tests). One series of inert gas tests was performed on a group of electro-deposited nickel screens containing uniform hole openings of from 2 to 7.5μ with length to diameter ratios (L/D) of from 1.6 to 5.6. The molecular flow conductance (rate of flow per unit difference of pressure between the ends of the channel) was calculated and also measured for these samples. Since the electro-deposited channels had conical entrance and exit sections, the flow rate would be expected to have a value between the flow predicted for a straight-sided channel having the minimum opening dimension and a zero-length orifice. Furthermore,

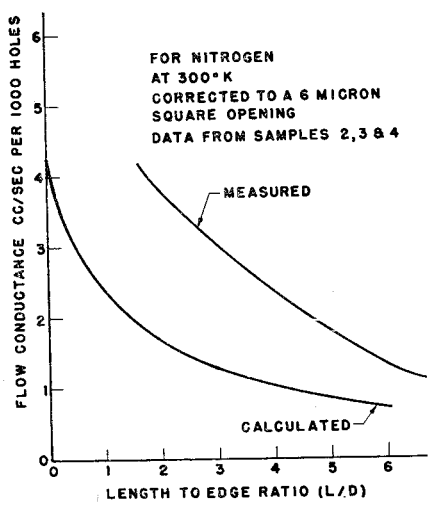

Fig. 2 Calculated and measured values of flow conductance vs L/D.

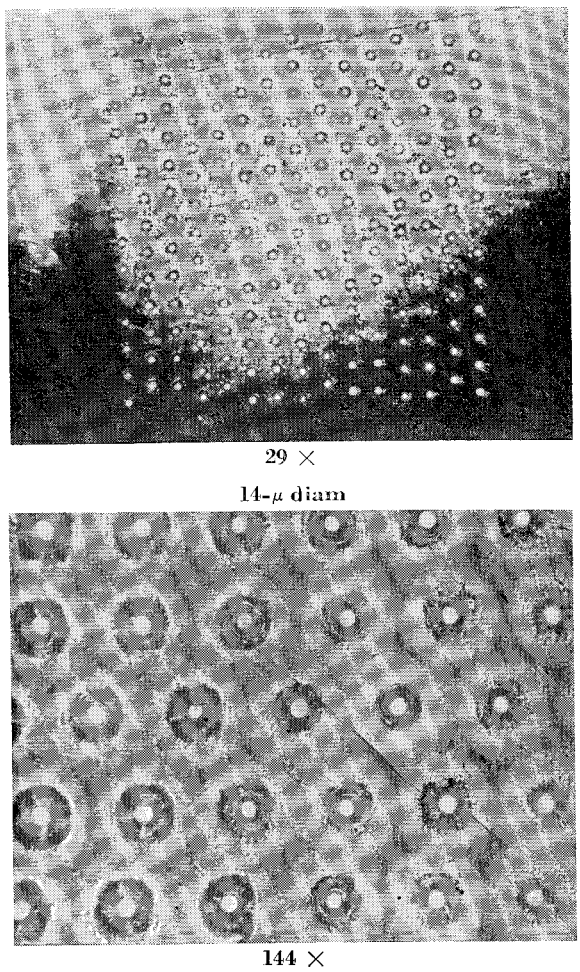

29 ×

14-μ diam

144 ×

Fig. 3 Electron beam-drilled tungsten emitter. Average hole diameter, 15 μ; edge-to-edge spacing, 85 μ.

it would be expected that the effect of the entrance and exit portions would be minimized as the channel length is increased. The test results are shown in Fig. 2. It is evident that for an L/D of about 2 (where L is taken as the sample thickness) sensibly orifice flow exists. As L/D is increased, the measured values more nearly approach the values calculated for the straight-sided channel.

Thus, the validity of calculation techniques (given by Ref. 4) was confirmed for this flow regime. Similar inert gas flow tests were used to establish a geometric correction factor for use in cesium flow calculations for the actual tungsten and molybdenum emitter samples. That is, the ratio of the measured flow conductance to the calculated flow conductance (assuming a cylindrical pore with a diameter equal to the minimum measured pore diameter) is used as a correction factor to account for the noncylindrical nature of the actual pore. The method used for these inert gas tests was a constant volume isothermal pressure decay technique, essentially as described in Ref. 2.

Cesium Flow Tests

Following inert gas flow testing, the emitters were subjected to high-temperature cesium flow tests to simulate actual operating conditions. After each cesium flow test, the hole diameter and nitrogen flow conductance were measured to determine effects of cesium flow. Hole diameters were measured on a metallurgical microscope using both back and front lighting. It was found that cesium had no apparent effect on hole size or emitter configuration. One electron beam-drilled emitter sample accumulated over 83 hr of cesium flow testing at 1200°C with no measurable change in hole size or flow conductance.[5]

During these flow tests, a measured amount of cesium was passed through the emitter for a known length of time at a constant value of cesium vapor pressure. A time-average cesium flow rate was obtained for each test. Comparison of this observed flow rate with the flow rate calculated for the same conditions and assuming only free molecular vapor flow showed that the measured flow rates were from 6 to 15 times the calculated values. Surface diffusion flow is to be expected in such a system, however. An indication of the relative magnitude of this surface diffusion component of flow is given in an analysis by Winterbottom and Hirth.[6] The ratio B of the surface diffusion component of flow to the molecular component is given by the expression

$$B = I_s/I_v = 2K_1(ER)/ERK_0(ER)$$

where

I_s = surface diffusion component of flow
I_v = molecular component of flow
$1/E$ = root mean square diffusion length on the surface = $(D_s\tau)^{1/2}$, where D_s is the surface diffusion coefficient, τ residence time of an atom on the surface, R radius of pore, and K_1 and K_0 are modified Bessel functions of the second kind of zero and first order, respectively.

Using the observed values of the system variables (pore radius, temperature) for a typical cesium flow test yields a calculated value of $B = 3.5$. The corresponding values of B based upon the observed time average cesium flow rate were $B = 5$ to $B = 14$. It should be noted that this value of $B = 3.5$ appears to represent a maximum figure, since a zero length orifice was assumed for this calculation. However, the values of D_s and τ under the actual operating conditions (i.e., the effects of surface contamination and crystallographic orientation) are not known with sufficient accuracy to draw a firm conclusion from this apparent anomaly. No other published data are known to the authors on cesium flow through small holes of fairly precise size and location.

Fabrication Techniques

A variety of fabrication processes was investigated in procuring the perforated emitters used for this study. The techniques included 1) laser drilling, 2) photoetching (chemical), 3) electron beam drilling, and 4) rotating mechanical drilling.

The laser demonstrated capability of drilling small holes in refractory metals. However, because of its early stage of development, insufficient uniformity or reproducibility was obtainable; therefore, laser samples were not tested.

Photoetching is a selective chemical etching process using photographic techniques to produce the image on the piece to be etched. Several samples made by this technique contained 1600 holes in the 15- to 20-μ diam range. These holes were etched in molybdenum 0.0005 in. thick. A large number of holes are made at one time; therefore, the process is relatively inexpensive. In addition, being basically a photographic reduction process, the master from which the screens are made can be many times the actual size, resulting in hole spacing controlled within very precise limits. On the other hand, present technology does not permit the use of tungsten in this process, and the target 10-μ diam is near the limit of the present state of the art. In this range, as the diameter is reduced, control of hole size also decreases. The largest single disadvantage of this process, however, is the apparent present limitation of $L/D = 1$, thus requiring very thin foils for small flow passages. It is possible, however, to reinforce such a thin foil with a thicker grid or mesh to provide mechancal strength.

Hole sizes as small as 2μ in diameter with an L/D of 3 can be obtained in some materials with the use of the rotating mechanical drill technique. The process obviously becomes more difficult when working with the refractory metals such as tungsten and molybdenum. Holes of 10μ have been made by this process in molybdenum sheets, but with considerable attendant dulling and breakage of the drills. However, when the same process was used to drill through and "clean-up" undersize holes previously made by the photoetch process, it was found that the technique was satisfactory. This can be a method of obtaining the desired hole sizes and dimensions, although the procedure remains a tedious one.

Table 1 Comparison of drilling methods

Method	Min. present hole diam, μ	Material	L/D
Laser	*[a]	Tungsten	*
Photoetch	10–20	Molybdenum	1
Mechanical drilling	2	Steel	3
	10	Molybdenum	3
Electron beam	12	Tungsten	10
Electro-deposit	2	Nickel	7

[a] An asterik indicates that the process is still under development and precise figures cannot be given.

The most promising fabrication technique to date has been a method of electron beam drilling. Figure 3 illustrates one of the earliest electron beam-drilled samples; hole size is 15μ spaced on 100-μ centers. The results to date indicate that small-diameter holes at a relatively high L/D are readily drilled in tungsten, with continuing progress being made in reducing hole size and spacing. For example, 12-μ-diam holes with 55-μ edge-to-edge spacing have been drilled in 0.005-in.-thick tungsten ($L/D = 10$). Diameter is quite reproducible, the present variation being $\pm 2\mu$ on a 12-μ diam. The process readily lends itself to automatic programming, thereby making it economically feasible to drill a large number of holes. (Although the holes are drilled singly, the drilling time per hole is approximately 0.5 sec.) In addition, groups of holes can be drilled at different locations in a large plate or emitter assembly, thus eliminating some of the usual welding or brazing operations associated with emitter mounting.

A comparison of the drilling methods is given in Table 1. It should be noted that these are initial results and that continued development of existing and new techniques is in process with the prospect of providing smaller holes with closer spacing.

Summary

Initial evaluation of perforated ion emitters under high-temperature cesium flow conditions indicates that little or no change of porosity with time was encountered. An electron beam-drilled emitter was run at 1200°C with cesium flow for 83 hr with no apparent change in hole size or flow conductance. In addition, the discrete and measurable pore openings (as opposed to the random passages in sintered emitters) permit calculations of emitter cesium flow rates. Typically, the calculated value of the ratio B was 3.5, whereas the observed value ranged from 5 to 14.

Of the various fabrication techniques investigated, electron beam drilling has provided the most satisfactory results to date with regard to reproducibility of hole size and spacing.

References

[1] Nazarian, G. M. and Shelton, H., "Theory of ion emission from porous media," *ARS Progress in Astronautics and Rocketry: Electrostatic Propulsion*, edited by D. B. Langmuir, E. Stuhlinger, and J. M. Sellen Jr. (Academic Press, New York, 1961), Vol. 5, pp. 91–106.

[2] Reynolds, T. W. and Kreps, L. W., "Gas flow, emittance, and ion current capabilities of porous tungsten," NASA TN D-871 (August 1961).

[3] Krauss, J. J. and Petrick, E. N., "Flow through small pore as applied to the design of ion emitters," AIAA Preprint 63040 (March 1963).

[4] Dushman, S., *Scientific Foundations of Vacuum Technique* (John Wiley and Sons Inc., New York, 1963), Chap. 2.

[5] Petrick, E. N. and Krauss, J. J., "The design and evaluation of perforated ion emitters" Final TR, Contract AF 33(657)-8638, performed for Aeronaut. Systems Div., U. S. Air Force, by Kelsey Hayes Co., Romulus, Mich. (September 15, 1963).

[6] Winterbottom, W. L. and Hirth, J. P., "Diffusional contribution to the total flow from a knudsen cell," J. Chem. Phys. **37**, 784–793 (1962).

Thermal Boundary Layer in Slip Flow Regime

K. C. Reddy*
Indian Institute of Technology, Kharagpur, India

VELOCITY-slip and temperature-jump boundary conditions replacing the classical conditions of no-slip and continuous temperature distribution have formed the basis of study of many a problem[1–5] in rarefied gas dynamics. First-order slip boundary conditions (neglecting thermal creep terms) are given by

$$u(x,0) = L(\partial u/\partial y)_{y=0} \tag{1.1}$$

$$T(x,0) - T_w = L_1(\partial T/\partial y)_{y=0} \tag{1.2}$$

where

$$L = \frac{2-f}{f}\lambda \qquad L_1 = \frac{2-f_1}{f_1}\frac{2\gamma}{\gamma+1}\frac{\lambda}{Pr}$$

f being the Maxwell's reflection coefficient, f_1 the thermal accommodation coefficient, λ the mean free path of the fluid at the surface, γ the specific heat ratio, Pr the Prandtl number, and T_w the wall temperature.

Putting

$$T - T_w = u^{L/L_1}\theta = u^\alpha\theta \tag{2}$$

where $\alpha = L/L_1$, the condition (1.2) reduces, on using (1.1), to the form

$$(\partial\theta/\partial y)_{y=0} = 0 \tag{3}$$

Thus the transformation (2) simplifies the temperature jump condition considerably. It is much easier to manage with condition (3) than its original form (1.2), particularly when Von Mises' transformation is used.

Hasimoto[2] has obtained a solution in power series of x to the boundary-layer momentum equation for the flow past a flat plate under slip conditions using Von Mises' transformation. Hassan[3] has extended this analysis to include the flows of a certain class of outer pressure distributions. In the present note, the author will follow Hassan's analysis to solve the corresponding energy equation using the transformation (2) and thus the simplified boundary condition (3). Two-dimensional incompressible boundary-layer momentum and energy equations are given by

$$uu_x + vu_y = VV_x + \nu u_{yy} \tag{4.1}$$

$$u_x + v_y = 0 \tag{4.2}$$

$$\rho c_p(uT_x + vT_y) = kT_{yy} + \mu(u_y)^2 \tag{4.3}$$

where V is the freestream velocity. Introducing the transformation (2), Eq. (4.3) becomes

$$\rho c_p\{u(u^\alpha\theta)_x + v(u^\alpha\theta)_y\} = k(u^\alpha\theta)_{yy} + \mu(u_y)^2 \tag{5}$$

The function θ should satisfy the condition (3) at the wall, and

$$\theta \to \frac{T_\infty - T_w}{V^\alpha} \quad \text{as } y \to \infty \tag{6}$$

where T_∞ is the freestream temperature. Taking (x,ψ), where ψ is the stream function, as independent variables instead of (x,y), Eq. (5) can be written as

$$(u^\alpha\theta)_x = \frac{\nu}{Pr}\{u(u^\alpha\theta)_\psi\}_\psi + \frac{\nu}{c_p}u(u_\psi)^2 \tag{7}$$

and the boundary conditions (3) and (6) reduce to

$$\theta_\psi = 0 \text{ at } \psi = 0 \qquad \theta \to \frac{T_\infty - T_w}{V^\alpha} \text{ as } \psi \to \infty \tag{8}$$

Introducing the dimensionless variables defined by

$$V = \frac{\nu}{L}h(\xi) \qquad \xi = \left(\frac{x}{L}\right)^{1/2} \qquad \eta = \frac{\psi}{\nu h}\left(\frac{L}{x}\right)^{1/2}$$

$$u = \frac{\nu}{L}h(\xi)\phi(\xi,\eta) \qquad \theta = \left(\frac{\nu}{L}\right)^{2-\alpha}\frac{g(\xi,\eta)}{c_p h^\alpha} \tag{9}$$

Eq. (7) takes the form

$$h\xi\frac{\partial}{\partial\xi}(\phi^\alpha g) - \left(h + \xi\frac{dh}{d\xi}\right)\eta\frac{\partial}{\partial\eta}(\phi^\alpha g) = \frac{2}{Pr}\frac{\partial}{\partial\eta}\left\{\phi\frac{\partial}{\partial\eta}(g\phi^\alpha)\right\} + 2h^2\phi\left(\frac{\partial\phi}{\partial\eta}\right)^2 \tag{10}$$

Correspondingly, the boundary conditions (8) are transformed to

$$\partial g/\partial\eta = 0 \text{ at } \eta = 0 \qquad g \to g_\infty \text{ as } \eta \to \infty \tag{11}$$

where

$$g_\infty = c_p(T_\infty - T_w)(L/\nu)^2$$

Following Hassan, assume series solutions for ϕ and g in powers of ξ, viz.,

$$\phi = 1 + \sum_{n=1}^{\infty}\phi_n(\eta)\xi^n \qquad g = g_\infty + \sum_{n=1}^{\infty}g_n(\eta)\xi^n \tag{12}$$

and suppose that h can be expanded into the form

$$h = \sum_{n=0}^{\infty}a_n\xi^n \qquad a_0 \neq 0 \tag{13}$$

Now consider the cases for $\alpha = 1$ and $\alpha = \frac{1}{2}$. It may be remarked that experimental and theoretical evidence[4] corresponds more to the latter case.

The Case of $\alpha = 1$

Substituting (12) and (13) into (10) and equating the coefficients of like powers of ξ, one obtains the equations for g_n as

$$g_n'' + \frac{Pr\,a_0}{2}(\eta g_n' - n g_n) = S_n(\eta) \tag{14}$$

where $S_n(\eta)$ involves $g_1, g_2, \ldots g_{n-1}, \phi_1, \ldots \phi_n$, their derivatives, and the constants $a_0, a_1, \ldots a_{n-1}$. Introducing the variables

$$G_n = \frac{Pr\,a_0}{4}g_n \qquad \zeta = \frac{(Pr\,a_0)^{1/2}}{2}\eta$$

Eq. (14) can be written as

$$G_n'' + 2(\zeta G_n' - nG_n) = S_n(\zeta) \tag{15}$$

where primes denote differentiation with respect to ζ.

Received April 22, 1963. This work is supported by the Council of Scientific and Industrial Research, Government of India in the form of a Junior Research Fellowship. The author wishes to record his deep sense of gratitude to Y. D. Wadhwa for his most helpful suggestions and guidance throughout the preparation of this note.

* CSIR Junior Research Fellow, Department of Mathematics.